Quantifying the Photoinduced Release of Nitric Oxide from *N,N′*-Bis(carboxymethyl)-*N,N′*-dinitroso-1,4-phenylenediamine. Effect of Reducing Agents on the Mechanism of the Photoinduced Reactions

Maria Zulema Cabail, Valerie Moua, Elisha Bae, Andrew Meyer, and A. Andrew Pacheco*

Department of Chemistry and Biochemistry, University of Wisconsin—Milwaukee, Milwaukee, Wisconsin 53211

Received: August 24, 2006; In Final Form: November 22, 2006

N,N′-Bis(carboxymethyl)-*N,N′*-dinitroso-1,4-phenylenediamine (**1**) fragments to release 1 equiv of NO• and the denitrosated radical of **1** (**2**), when exposed to a ∼10 ns, 308 nm laser pulse. Species **2** can fragment to give another equivalent of NO• and the doubly denitrosated quinoimine derivative of **1** (**3**), it can recombine with NO• to give **1** and ring-nitrosated isomers of **1**, or in the presence of a reducing agent, **2** can be reduced (to species **4**). Photogenerated NO• can be used to probe fast reactions of biochemical interest, making **1** a valuable research tool. This paper focuses on the chemistry of **2**, whose reactivity must be well characterized if **1** is to be used to its full potential. $[Ru(NH_3)_6]^{2+}$ (Ru^{II}) and $[Fe(CN)_6]^{4-}$ (Fe^{II}) were both shown to reduce **2**, with bimolecular rate constants in the diffusion limit. When solutions initially containing 70 μM of Ru^{II}, 20 μM myoglobin (Mb) and varying amounts of **1** were irradiated, the only Mb reaction product was nitrosomyoglobin (MbNO). In contrast, in solutions containing only Mb and **1**, Mb is converted to both MbNO and oxidized myoglobin (metMb). When Fe^{II} was used in place of Ru^{II}, Mb was oxidized to metMb, but ∼100× more slowly than in solutions containing only Mb and **1**. This showed that **2** first oxidized Fe^{II} to $[Fe(CN)_6]^{3-}$ (Fe^{III}), which then oxidized Mb at the slower rate. The ratio metMb/MbNO obtained in the experiments with Fe^{II} was 0.6, whereas the ratio predicted from previously known chemistry of **2** was ∼1 under the experimental conditions. The result is explained if, upon photolysis, **1** first forms a caged encounter complex [**2**, NO•], which fragments to give **3** and 2 equiv of NO•, without ever releasing free **2** into solution. This hypothesis was further strengthened by analyzing the amount of NO• generated by photolysis of **1** in the absence of added reductant. The original mechanism underestimates the NO• generated, a problem solved by invoking direct release of NO• and **3** from photolysis of **1**.

1. Introduction

The compound *N,N′*-bis(carboxymethyl)-*N,N′* -dinitroso-1,4-phenylenediamine (**1**) has been shown to release NO• upon photoactivation with 308 nm light.[1−5] NO• is now known to play numerous important roles in human physiology,[6−13] and this has provided the primary driving force for synthesizing compounds such as **1**, that are biologically inert but could potentially be activated to release NO• once they reach specific biological target sites.[1,3,14−16] Though initially designed for NO• release in potential biomedical applications,[1−3] in our hands **1** is also proving to be a valuable tool for in vitro research.[17,18] In this research we use the photogenerated NO• as a probe for studying metalloprotein reactions that feature, at least formally, metal-bound NO• species as intermediates. NO• can be generated from **1** in less than 1 μs using a XeCl excimer laser, so very fast subsequent reactions of NO• with other compounds can then be monitored.[1,5,17] Furthermore, the concentration of NO• within a given experiment is readily controlled, either by varying the intensity of the laser pulse or by maintaining the laser pulse constant and varying the concentration of **1**.[4] For our purposes it is important to know, as accurately as possible, the concentration of NO• that is generated from **1** under any given set of conditions. Furthermore, before **1** can be confidently used as a NO• generator for probing the reactivity of metalloproteins, one must rule out the existence of side-reactions that **1**, or products generated by its photolysis, might undergo with the metalloproteins of interest. These considerations led us to do a detailed mechanistic investigation of the photochemistry of **1** that is still ongoing. Herein we report the latest results of this investigation.

Scheme 1 shows the major reactions that are believed to follow irradiation of **1**.[1,5,17] The laser pulse promotes the fragmentation of **1** into **2** and NO• (Scheme 1, eq 1). Species **2** is very reactive and will rapidly recombine with NO• (eq 1 back-reaction), or fragment further to give the relatively stable species **3** and a second equivalent of NO• (Scheme 1, eq 2). More recently, species **2** was shown to be a powerful oxidant,[5] which is irreversibly reduced to **4** in the presence of a suitable electron donor (Scheme 1, eq 3). In addition to the primary reaction pathways of Scheme 1, several minor pathways appear to become available due to recombination of NO• with **2** at either the ortho or para position of the phenyl ring.[5] Such recombination processes would give rise to metastable ring-nitrosated species, instead of regenerating **1**, as suggested by the back-reaction of Scheme 1, eq 1.

The initial motivation behind the study reported herein was to develop protocols for using **1** as a NO• generator, in the presence of metalloproteins that are also electron donors. Generally, one will be interested only in the nitrosylation of a given metalloprotein, and concomitant oxidation of this protein by **2** (Scheme 1, eq 3) will be undesirable. Our plan was to add a sacrificial electron donor to the mixture of **1** and enzyme, which

* To whom correspondence should be addressed. E-mail: apacheco@uwm.edu.

10.1021/jp065487y CCC: $37.00
Published on Web 02/01/2007

SCHEME 1: "Red" in Eq 3 Refers to an Arbitrary Electron Donor

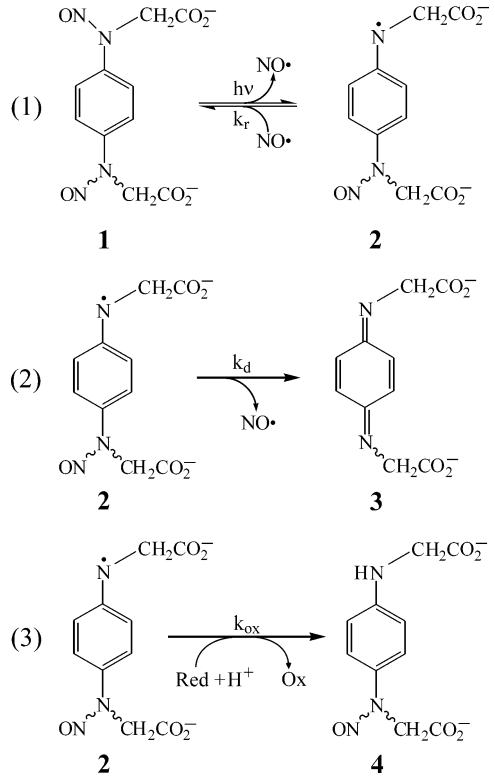

would reduce species 2 orders of magnitude faster than the test protein could. In this regard, $[Ru(NH_3)_6]^{2+}$ and $[Fe(CN)_6]^{4-}$ both proved to be suitable donors. Furthermore, as will be shown below, important new insights into the photochemistry of **1** were obtained while developing the protocols that use $[Ru(NH_3)_6]^{2+}$ and $[Fe(CN)_6]^{4-}$ as sacrificial electron donors.

2. Experimental Section

2.1. Materials. The synthesis of the photoactive NO• releasing species **1** has been described elsewhere.[4] $[Ru(NH_3)_6]Cl_2$ was obtained from Aldrich, and $K_4[Fe(CN)_6]\cdot 3H_2O$ from Acros Organics. Myoglobin (crystallized and lyophilized horse skeletal muscle) was obtained from Sigma in the fully oxidized ferric form, known as met-myoglobin (metMb). For experiments requiring ferromyoglobin (Mb), the ferric protein was reduced by titrating it with exactly 1 equiv of Ti(III) citrate.[19] All photochemical experiments were performed in solutions buffered with phosphate ($F = 50$ mM, pH = 7.4). Stock solutions were prepared daily in a nitrogen filled glovebox and stored in a fridge at 4 °C until needed.

2.2. Data Collection and Instrumentation. Routine UV/vis spectra were obtained using a CARY 50 spectrophotometer (Varian), which was installed in the glovebox. Photochemical fragmentation of species **1** was initiated with a 10 ns, 308 nm, 6.0 mJ pulse from a XeCl excimer laser (TUI, Existar 200). An OLIS RSM-1000 spectrophotometer was used to monitor the absorbance changes induced by the laser pulse. The configuration of the laser and spectrophotometric equipment has been described in general terms elsewhere,[4] and some additional details are provided as Supporting Information. Most data were collected with the OLIS RSM-1000 in rapid-scanning mode (scanning slit width = 0.2 mm), which allows complete spectra to be obtained in 1 ms. An exception are the data shown in Figure 1, which were collected with the spectrophotometer in fixed-wavelength mode (fixed middle slit width = 0.6 mm). In this mode changes in absorbance at a single wavelength could be obtained for time intervals as short as 1 μs. For the fixed wavelength experiments the samples were held in 2 mm × 10 mm fluorescence cuvettes, and the incoming laser pulses were attenuated with a filtering solution of **1** with absorbance 1, as described in ref 4. For all other experiments the solutions were held in 3 mm × 3 mm fluorescence cuvettes, which were irradiated with unattenuated laser pulses, as described in ref 18. For both the fixed-wavelength and rapid-scanning experiments, the monochromator entrance slit width was 0.6 mm, and the exit slit width was 0.12 mm. The 418.7 nm band of holmium oxide (IBM Standards 9420) was used as a reference for calibrating the spectrophotometer wavelength in each mode.

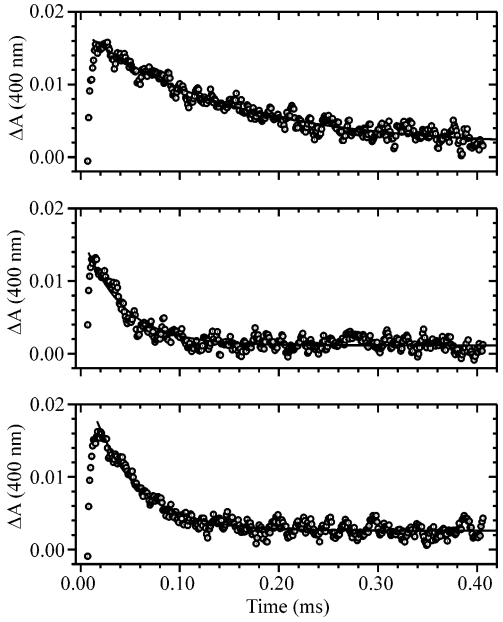

Figure 1. (a) Changes in absorbance at 400 nm observed after a solution containing **1** is irradiated with a 10 ns, 308 nm laser pulse (6 mJ, attenuated by 90% with a filtering solution of **1**; ref 4). (b) Same as (a), but the irradiated solution also contained 9.0 μM of $[Ru(NH_3)_6]^{2+}$. (c) Same as (a), but the irradiated solution also contained 25.2 μM of $[Fe(CN)_6]^{4-}$. Single-exponential fits are overlayed on each of the three experimental traces. Traces obtained at other $[Ru^{II}]$ and $[Fe^{II}]$, along with analyses of the k_{obs} dependence on $[Ru^{II}]$ and $[Fe^{II}]$, are available as Supporting Information.

2.3. Data Analysis. Data were analyzed using the commercially available software packages Specfit/32, Version 3.0 (Spectrum Software Associates), Microcal Origin, Version 6.0 (Microcal Software, Inc.) and Mathcad 11 (Mathsoft Engineering and Education, Inc.). Complete spectra obtained using the Olis RSM were first subjected to singular value decomposition (SVD) to determine the number of colored species, and to decrease the noise in the matrix of absorbances.[20] A matrix form of Beer's law (eq 1′) was then used to calculate the concentrations of all species in solution as a function of time.[20,21] In eq 1′ **A** is an absorbance matrix (after cleaning up by SVD), in which each row corresponds to a spectrum, and each column to a time trace at a fixed wavelength; ϵ is the matrix of extinction coefficients, in which each row corresponds to a unique species, and each column to a wavelength; **C** is the matrix of concentrations, in which each column corresponds to a unique species, and each row to a specific time; and l is a scalar representing the path length.

$$\mathbf{C} = (1/l)(\mathbf{A})\cdot\epsilon^{T}\cdot(\epsilon\cdot\epsilon^{T})^{-1} \qquad (1')$$

A value of $l = 5$ mm was used in experiments incorporating 2 mm × 10 mm cuvettes, and one of $l = 2.55$ mm was used in

conjunction with 3 mm × 3 mm cuvettes (see Supporting Information). The extinction coefficients for ϵ were obtained as follows. For metMb reliable extinction coefficients are available at specific wavelengths,[22] and these were used to determine the concentrations of metMb stock solutions. These concentrations were subsequently used to calculate the complete ϵ value spectrum of the protein. With the ϵ-value spectrum of metMb in hand, the protein was fully reduced with Ti(III) to obtain the ϵ-value spectrum of Mb. Finally, stock solutions of Mb and metMb were put under NO• to obtain ϵ-value spectra of MbNO and metMbNO, respectively.

3. Results and Discussion

3.1. Effect of $[Ru(NH_3)_6]^{2+}$ on [NO•] Output after Photolysis of Species 1. Figure 1a shows how the 400 nm absorbance of a solution, initially containing only species **1**, changes after being irradiated with a 308 nm, 10 ns laser pulse, that has first been attenuated with a filter of absorbance 1.[4] Species **2** (Scheme 1) has an absorbance maximum at 400 nm, and the trace in Figure 1a tracks the appearance and subsequent disappearance of this intermediate.[1,5,17] ΔA_{400} reaches a maximum immediately after the laser pulse, and then decreases as **2** is consumed by the reactions of Scheme 1. Notably, addition of 9 μM $[Ru(NH_3)_6]^{2+}$ to the reaction mixture prior to irradiation by the laser pulse, substantially increases the subsequent rate of disappearance of **2** (Figure 1b). This suggests that $[Ru(NH_3)_6]^{2+}$ can reduce **2** as shown in Scheme 1, eq 3.

Equations 2′ and 3′ are the expected rate equations for **2** and NO•, based on the mechanism of Scheme 1. In eq 2′, $[Ru(NH_3)_6]^{2+}$ is abbreviated as Ru^{II}. For reactions in which no $[Ru^{II}]$

$$\frac{d[\mathbf{2}]}{dt} = (k_r[NO^\bullet] + k_d + k_{ox}[Ru^{II}])[\mathbf{2}] \qquad (2')$$

$$\frac{d[NO^\bullet]}{dt} = (k_d - k_r[NO^\bullet])[\mathbf{2}] \qquad (3')$$

was added, the bracketed term in eq 2′ simplifies to (k_r[NO•] + k_d). Interestingly, despite the presence of the k_r[NO•] term in eq 2′, the disappearance of **2** is readily modeled using a single exponential, except when the amount of **2** initially generated by the laser pulse is very high. This can be seen both in Figure 1a (no added reductant) and in Figure 1b,c, in which reductants were added to the reaction mixture prior to photoirradiation. A detailed explanation for this phenomenon was provided in an earlier paper.[4] However, one can readily obtain a qualitative understanding by noting from eq 3′ that if k_r[NO•] = k_d immediately after the laser pulse (i.e., at $t \approx 0$), then d[NO•]/dt will remain zero at all t, and [NO•] will remain constant at $[NO^\bullet]_0$. In practice it can be shown that [NO•] remains *fairly* constant even if $k_r[NO^\bullet]_0 \neq k_d$, but the two terms are not too different.[4] This allows one to define an approximate rate constant, $k_0 \approx (k_r[NO^\bullet] + k_d)$, and to write the bracketed term of eq 2 as ($k_0 + k_{ox}[Ru^{II}]$). If only a small fraction of $[Ru^{II}]_0$ reacts with [**2**], then the entire bracketed term will be a pseudo-first-order rate constant k_{obs}. This will be true when $[Ru^{II}]_0 \gg [\mathbf{2}]_0$, but it will also be true at lower $[Ru^{II}]_0$, because then oxidation of [**2**] will be a minor pathway compared to recombination with NO•, and fragmentation to generate **3**.

The experiments shown in Figure 1 were analyzed using the reasoning from the previous paragraph, and from this analysis the value of k_{ox} was calculated to be (2.1 ± 0.1) × 10^9 M^{-1} s^{-1} for the reduction of **2** by Ru^{II} (see Supporting Information). This value is 2 times larger than that determined earlier for k_r

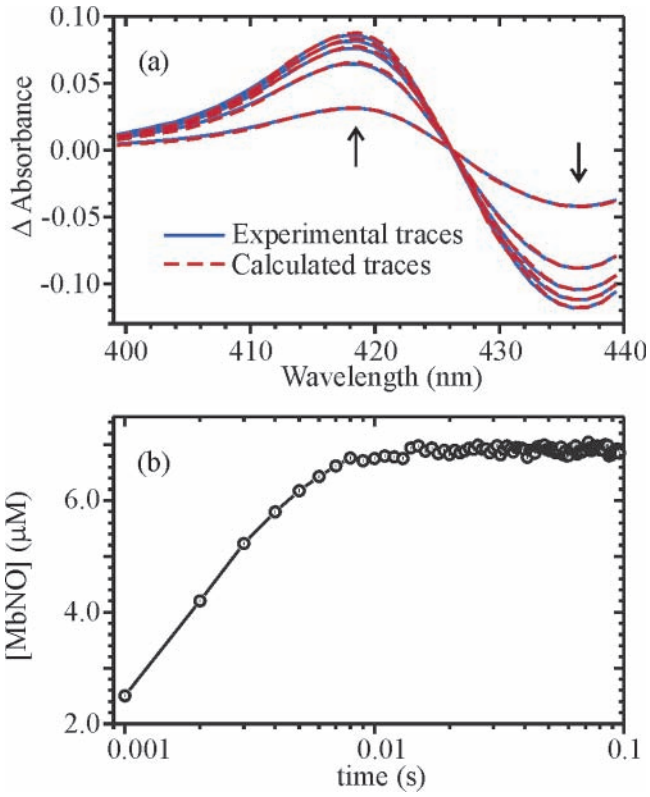

Figure 2. (a) Spectral changes (blue) observed after a solution containing 22.1 μM Mb, 75.5 μM $[Ru(NH_3)_6]^{2+}$, and 15.7 μM **1**, is irradiated with a 10 ns, 308 nm laser pulse. The representative difference spectra shown here were collected 1, 3, 5, 7 and 30 ms after the laser pulse. Theoretical traces (red dashed) were calculated from the known extinction coefficients of Mb and MbNO, as described in the Experimental Section. (b) [MbNO] vs time trace corresponding to the data shown in (a). Data sets obtained under different conditions are provided as Supporting Information.

(1.1 ± 0.1) × 10^9 M^{-1} s^{-1} [4] and is essentially at the diffusion limit for bimolecular reactions.[23] This makes $[Ru(NH_3)_6]^{2+}$ an excellent candidate to act as a sacrificial electron donor for protecting proteins of interest from reduction by **2**. The methodology was first tested on Mb, whose reactivity with NO• has been extensively documented in previous investigations.[24,25] When solutions containing **1** and Mb were irradiated in the presence of $[Ru(NH_3)_6]^{2+}$, the only reaction undergone by Mb was nitrosylation to give MbNO (Figure 2). Irradiation of solutions containing **1** and Mb, but no other reducing agent, leads to both nitrosylation and oxidation of Mb by **2**.[5] Thus, it appears that $[Ru(NH_3)_6]^{2+}$ rapidly reduces species **2** to **4** (Scheme 1, eq 3), before **2** can oxidize Mb instead. This was the desired result.

Mb reacts quantitatively with NO•.[25] Thus, the [MbNO] that is present after traces such as Figure 2b level out ($[MbNO]_f$), is numerically equal to the amount of [NO•] that results from photolysis of **1** and is not scavenged by recombination with **2**. Figure 3 shows a plot of $[MbNO]_f$ vs [**1**] initially added to the reaction mixture ($[\mathbf{1}]_{tot}$). The plot is essentially linear until $[MbNO]_f$ = 22 ± 1 μM, beyond which point $[MbNO]_f$ = $[Mb]_{tot}$, the total amount of Mb initially added to the reaction mixture. The fact that all of the Mb can be converted to MbNO at sufficiently high $[\mathbf{1}]_{tot}$, together with the extremely good fit of the Figure 2a data that was obtained using only the $\epsilon_{MbNO} - \epsilon_{Mb}$ standard difference spectrum, shows that Mb does not undergo any side reactions under the experimental conditions. With $[\mathbf{1}]_{tot}$ fixed anywhere in the linear range, the $[Ru(NH_3)_6]^{2+}$ concentration could be varied from 50 μM to 1 mM without significantly affecting the $[MbNO]_f$. The logical explanation is

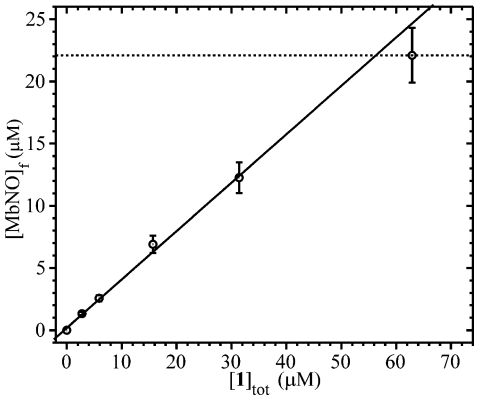

Figure 3. Plot of $[MbNO]_f$ vs [**1**] initially added to the reaction mixture ($[\mathbf{1}]_{tot}$), when $[Ru(NH_3)_6]^{2+}$ is used as a sacrificial electron donor. The concentration of $[Ru(NH_3)_6]^{2+}$ was 75.5 μM in every case. The dotted line represents $[Mb]_{tot}$, the concentration of Mb initially present in solution. In this and other figures, the error bars are set at ±10% of any given [MbNO] value. This uncertainty was estimated from experiments in which multiple replicates were obtained under identical conditions.[18] The major sources of error are believed to be the variations of laser pulse intensity and $[Mb]_{tot}$ from one experiment to the next (see also Supporting Information).[18]

that under these reaction conditions, virtually all of species **2** was reduced to **4** (Scheme 1, eq 3) before it could recombine with NO• (Scheme 1, eq 1), or fragment to give NO• and **3** (Scheme 1, eq 2). This explanation will later be slightly modified to accommodate the results presented in the next sections; however, numerical simulation of the Scheme 1 reactions, using the known parameters $k_r = (1.1 \pm 0.1) \times 10^9$ M^{-1} s^{-1},[4] $k_d =$ 2500 s^{-1},[5] and $k_{ox} = (2.1 \pm 0.1) \times 10^9$ M^{-1} s^{-1}, shows that the explanation is essentially correct.

3.2. Effect of $[Fe(CN)_6]^{4-}$ on [NO•] Output after Photolysis of Species 1. Further experiments showed that $[Fe(CN)_6]^{4-}$ is also a competent sacrificial electron donor that reduces **2** only slightly more slowly than $[Ru(NH_3)_6]^{2+}$ under comparable conditions (Figure 1c). The value of k_{ox} for $[Fe(CN)_6]^{4-}$ was determined to be $(6.3 \pm 0.3) \times 10^8$ M^{-1} s^{-1} (see Supporting Information), which is roughly one-third of the value for $[Ru(NH_3)_6]^{2+}$, and only slightly below k_r for recombination of **2** with NO• (Scheme 1, eq 1).[4] A new feature is that when the experiments with Mb are repeated with $[Fe(CN)_6]^{4-}$ replacing $[Ru(NH_3)_6]^{2+}$, oxidation of Mb to metMb accompanies nitrosylation of Mb to MbNO (Figure 4). Interestingly, the oxidation process is significantly slower than nitrosylation (Figure 4b); when **1** and Mb are irradiated under comparable conditions, but in the absence of any reductant, Mb oxidation is faster than Mb nitrosylation.[5] It appears that the Mb oxidation seen in Figure 4 is effected by $[Fe(CN)_6]^{3-}$, as suggested in Scheme 2. Ferricyanide ($[Fe(CN)_6]^{3-}$) is a well-known oxidizing agent, with a standard reduction potential of 360 mV.[26] By comparison $E°$ is 100 mV for $[Ru(NH_3)_6]^{3+}$,[26] and 46 mV for metMb.[27] Notice that, according to Schemes 1 and 2, the final concentration of metMb ($[metMb]_f$) provides a direct measure of the amount of **2** that was reduced by $[Fe(CN)_6]^{4-}$, just as $[MbNO]_f$ measures the amount of free NO• that escaped recombination. Finally, note that at sufficiently high $[\mathbf{1}]_{tot}$, the mixture of MbNO and metMb accounts for all of the Mb initially added to the solution. Together with the extremely good fit of the Figure 4a data that was obtained using only the $\epsilon_{MbNO} - \epsilon_{Mb}$ and $\epsilon_{metMb} - \epsilon_{Mb}$ standard difference spectra, this result shows that Mb oxidation and nitrosylation are the only protein reactions under the experimental conditions.

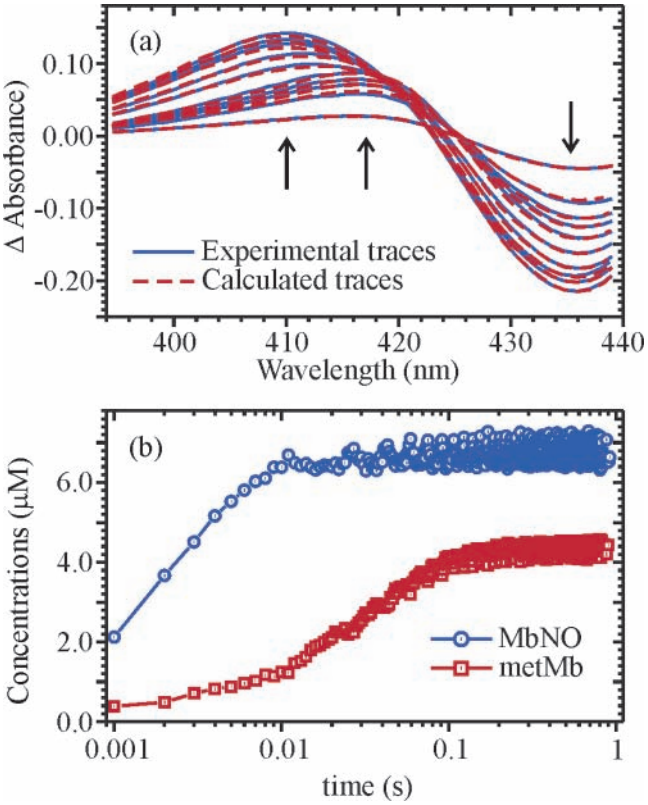

Figure 4. Spectral changes (blue) observed after a solution containing 21.7 μM Mb, 70 μM $[Fe(CN)_6]^{4-}$, and 15.7 μM **1**, is irradiated with a 10 ns, 308 nm laser pulse. The representative difference spectra shown here were collected 1, 3, 5, 7, 11, 21, 41, 61, 81 and 201 ms after the laser pulse. Theoretical traces (red dashed) were calculated from the known extinction coefficients of Mb, metMb and MbNO, as described in the Experimental Section. (b) [MbNO] and [metMb] vs time traces corresponding to the data shown in (a).

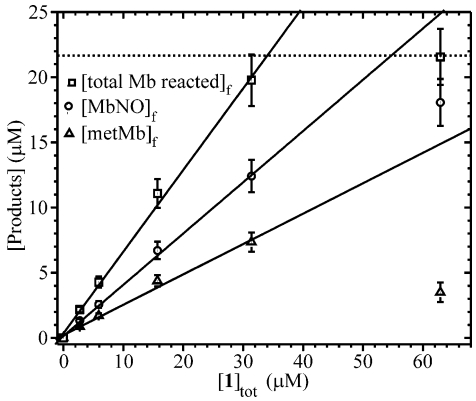

Figure 5. Plots of $[MbNO]_f$, $[metMb]_f$ and [total Mb reacted]$_f$ vs $[\mathbf{1}]_{tot}$, when $[Fe(CN)_6]^{4-}$ is used as a sacrificial electron donor. The concentration of $[Fe(CN)_6]^{4-}$ was 70 μM in every case. The dotted line represents $[Mb]_{tot}$.

SCHEME 2

$$\mathbf{2} + [Fe(CN)_6]^{4-} \xrightarrow[(fast)]{k_{ox}} \mathbf{4} + [Fe(CN)_6]^{3-} \quad (4)$$

$$[Fe(CN)_6]^{3-} + Mb \xrightarrow[(slow)]{k_{ox2}} [Fe(CN)_6]^{4-} + metMb \quad (5)$$

As is the case when $[Ru(NH_3)_6]^{2+}$ is the sacrificial electron donor, plots of $[MbNO]_f$ vs $[\mathbf{1}]_{tot}$ at fixed $([Fe(CN)_6]^{4-})_{tot}$ are linear until $([MbNO]_f + [metMb]_f) = [Mb]_{tot}$ (Figure 5). Indeed, the linear fits in both cases were found to have identical slopes (0.39 ± 0.1) over a wide range of sacrificial donor concentrations. Figure 5 shows that the plot of $[metMb]_f$ vs $[\mathbf{1}]_{tot}$ is also

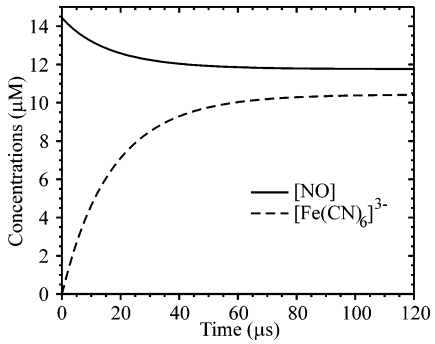

Figure 6. Simulated traces of [NO•] and [Ox] as a function of time, obtained by numerically integrating eqs 2 and 3 (and corresponding equations for d[Ox]/d*t* and d[Red]/d*t*), using Mathcad's Rkadapt algorithm. The values of k_r and k_d are those of refs 4 and 5, and 6.3×10^8 was used as k_{ox} for $[Fe(CN)_6]^{4-}$ (see text). Initial conditions: $[NO]_0 = [\mathbf{2}]_0 = 14.4\ \mu M$; $[Red]_0 = 70\ \mu M$. The calculated $[NO^\bullet]_f = 11.8\ \mu M$, which on the basis of Figure 5 would correspond to $[\mathbf{1}]_{tot} = 30\ \mu M$ (This assumes that $[MbNO]_f$ from Figure 5 corresponds to $[NO^\bullet]_f$ from the simulation). Calculated $[Ox]_f/[NO^\bullet]_f = 0.89$.

linear until $([MbNO]_f + [metMb]_f) = [Mb]_{tot}$. However, the $[metMb]_f$ obtained at any given [**1**] is only 60% of the $[MbNO]_f$ generated under the same conditions, even though Mb is the only species in solution that can be oxidized by the $[Fe(CN)_6]^{3-}$. This is also clearly seen in Figure 4, but the result is not consistent with the model proposed in Schemes 1 and 2, given the reaction conditions, as will now be demonstrated. Figure 6 shows simulated traces for [NO•] and [Ox] as a function of time, obtained by numerically integrating eqs 2 and 3 (and the corresponding equations for d[Ox]/d*t* and d[Red]/d*t*). Notice that the calculated final ratio of $[Fe(CN)_6]^{3-}$ to [NO•] ($[Ox]_f/[NO^\bullet]_f$) is 0.89, which is significantly higher than the 0.6 ratio for $[metMb]_f/[MbNO]_f$ seen in Figures 4 and 5. The simulation is fairly insensitive to the initial values chosen for [NO•] and [**2**], and ($[Ox]_f/[NO^\bullet]_f$) drops to 0.6 only when $[Red]_{tot}$ drops to 15 μM. Furthermore, the ratio stays above 0.8 until $[Red]_{tot} = 38\ \mu M$; recall that in the experiments being described $([Fe(CN)_6]^{4-})_{tot}$ was 70 μM.

At present we cannot give a definitive explanation for the discrepancy between the theoretical and observed ratios of oxidation to nitrosylation, but Scheme 3 presents some possibilities that would account for the data. All of the proposed explanations start from the hypothesis that NO• can somehow be liberated from **1** through processes that do not generate free **2** in solution. The simplest explanation is that, upon photolysis, the caged encounter complex of **2** and NO• can further fragment to produce species **3** and 2 equiv of NO• directly (the process governed by k_{d2} in Scheme 3). The second fragmentation could be assisted by direct attack of the photodissociated NO• on the still bound RNO, a process that would initially produce free N_2O_2, as shown in Scheme 3. N_2O_2 is not stable at room temperature[28] and so should rapidly dissociate into 2 equiv of NO•.

Scheme 3 also presents a second pathway for generating NO• without producing free **2**, via a metastable cage recombination species (**1c** in Scheme 3). A straightforward electron pushing analysis of the radical intermediate **2** suggests that the unpaired electron is probably significantly delocalized, putting spin density on the ortho and para carbons of the phenyl ring (Scheme 3, species **2b** and **2c**), in addition to the amine group (species **2a**). If there is indeed significant spin delocalization from the nitrogen to the ortho and para carbons of the intermediate, then in the NO•-recombination reaction the incoming NO• could reattach at either of these carbons, to give the metastable species

SCHEME 3

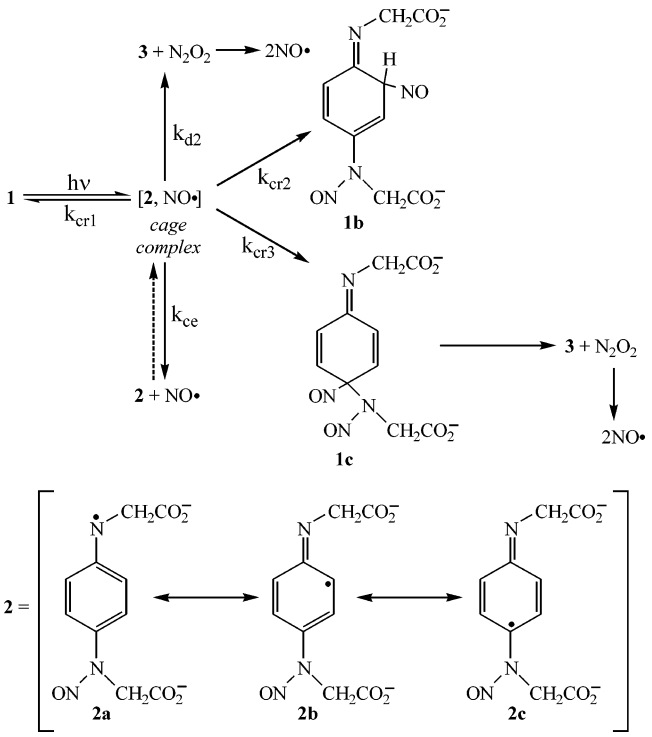

1b or **1c** instead of **1** (Scheme 3). Some evidence was presented in an earlier paper that species **1b** undergoes tautomerization on the millisecond time scale to give the aromatic, *o*-nitrosated isomer of **1**.[5] Species **1c** cannot tautomerize, but we speculate that the vicinial nitroso groups could dissociate as N_2O_2, generating species **3** in the process (Scheme 3). The key feature of both the direct release and **1c**-mediated mechanisms is that they would allow NO• to be generated via a process other than k_{ce}. As shown earlier, when $[Red]_0$ is large the predominant reaction of **2** is expected to be reduction to **4**, which would result in roughly equivalent amounts of NO• and [Ox] (Figure 6). By generating NO• directly without releasing free **2**, the two alternative processes provide mechanisms for generating "extra" equiv of NO•, without concomitant generation of Ox.

3.3. Measurement of the [NO•] Output after Photolysis of Species 1, in the Absence of a Sacrificial Electron Donor. For these experiments Mb could not be used as a NO• scavenger, because the protein itself can act as an electron donor.[5] Instead, metMb was used as the scavenger. Unlike Mb, metMb binds NO• weakly, with an equilibrium constant $K_{NO} = 2400\ M^{-1}$.[22] Nevertheless, from the equilibrium expression, the amount of NO• generated under any given set of conditions could be measured by calculating $[metMbNO]_f$ from the difference spectra following photolysis of **1** (see Supporting Information).

Initially, the results of irradiating mixtures of metMb, **1** and $[Fe(CN)_6]^{4-}$ were compared with those obtained earlier for mixtures of Mb, **1** and $[Fe(CN)_6]^{4-}$. Both methods should yield the same relationship for [NO•] generated as a function of $[\mathbf{1}]_{tot}$ in solution, so these experiments provided a means of checking the results of the two analytical methods against each other. In addition, because binding of NO• to metMb is so weak, only a small fraction of the total [NO•] ever binds to metMb under a given set of conditions. Hence, this method allowed us to check the [NO•] generated for solutions containing very high initial concentrations of **1**, which would have resulted in 100% nitrosylation of Mb. Figure 7 shows the results of these experiments; a systematic error has been corrected for in the figure, as explained in the Supporting Information. As can be

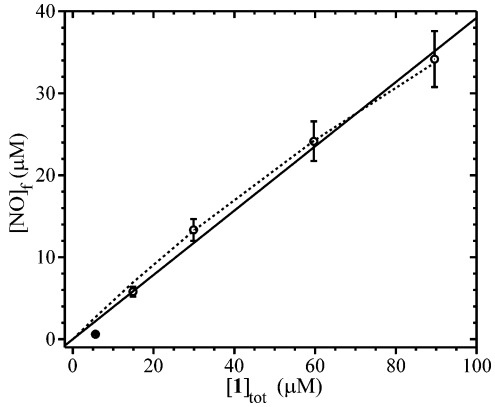

Figure 7. Amount of NO• generated as a function of $[\mathbf{1}]_{tot}$ in solution, in the presence of $[Fe(CN)_6]^{4-}$, as calculated using metMb as the NO• sensor. [metMb] = 18.4 μM; $[Fe(CN)_6]^{4-}$ = 77 μM. Circles: experimental data. Solid line: net [NO•] release predicted from the results of the Mb experiments, using the linear relationship $[NO^{\bullet}] = 0.39[\mathbf{1}]_{tot}$. Dotted line: net [NO•] release predicted using the mechanistic model of Scheme 4.

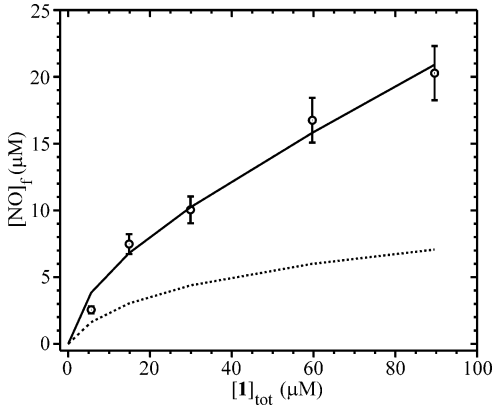

Figure 8. Total amount of NO• generated as a function of $[\mathbf{1}]_{tot}$ in solution, in the absence of any external electron donor, calculated using metMb as the NO• sensor. [metMb] = 17.7 μM. Circles: experimental data. Solid line: data simulated using the mechanism of Scheme 4, as described fully in Supporting Information. Dotted line: data simulated using the mechanism of Scheme 1.

seen, a plot of [NO•] generated vs $[\mathbf{1}]_{tot}$ is almost linear, with a calculated slope identical to that predicted from the experiments with Mb. The data do show a very slight curvature. This is readily explained because with high concentrations of **1**, higher concentrations of NO• are generated, and recombination of NO• with **2** (Scheme 1 eq 1) begins to compete with the reduction of **2** (Scheme 1, eq 3). As will be shown below, a more sophisticated treatment of the data using the known values of k_r, k_d[4,5] and k_{ox}, allows the curvature to be modeled (dashed curve in Figure 7). Note however, that although the more elaborate treatment provides valuable mechanistic insights, it is no better than the linear treatment for empirical prediction of the amount of NO• generated as a function of $[\mathbf{1}]_{tot}$.

Figure 8 shows the results obtained when solutions containing metMb and **1** in the absence of any sacrificial reductant were irradiated with 308 nm laser pulses. In this case, Scheme 1 predicts that the amount of NO• generated will be governed by the Scheme's reactions 1 and 2. In two earlier papers we estimated the values of k_r and k_d to be $(1.1 \pm 0.1) \times 10^9$ M^{-1} s^{-1} [4] and 2600 ± 100 s^{-1},[5] respectively. However, the values of [NO•] as a function of $[\mathbf{1}]_{tot}$ that were computed using these numbers significantly underestimated the experimental [NO•] generated (Figure 8). Interestingly, this result proves to be consistent with the results presented in Section 3.2. There we found that $[MbNO]_f \neq [metMb]_f$ when mixtures of Mb, **1** and $[Fe(CN)_6]^{4-}$ are irradiated, which is also contrary to the prediction of Scheme 1. In that situation we proposed that some "extra" NO• was generated through processes that did not generate free **2** in solution, as shown in Scheme 3. Such processes might also explain why the amount of NO• generated in the absence of an added reducing agent exceeds that predicted by Scheme 1 alone.

SCHEME 4

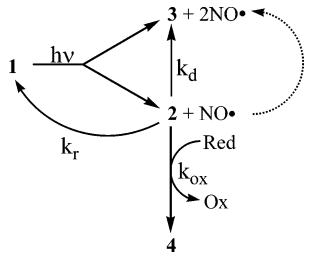

The experiments performed to date in our laboratories provide no direct information about the putative cage complex of **2** and NO•, or its reactions, so there is no way to meaningfully test the predictions of Scheme 3 numerically. Instead, we used a highly simplified mechanistic model (Scheme 4), to test the effect of having a pathway by which free NO• can be photogenerated without concomitant production of free **2**. The reaction pathways shown in Scheme 4 are identical to those of Scheme 1, except that the initial photochemical reaction is presumed to generate some **3** + 2NO• directly, in addition to forming **2** + NO•. Because all of the rate constants for the Scheme 4 process are known, it can be readily modeled using numerical integration (Supporting Information). In the integration process the initial concentrations of **2** and NO• (their concentrations immediately following the laser pulse, which we refer to as $[\mathbf{2}]_0$ and $[NO^{\bullet}]_0$) were treated as adjustable parameters, and the initial concentrations of the remaining species were constrained by stoichiometric considerations. The Scheme 4 model was used to simulate the data of both Figure 7 (dashed curve) and Figure 8 (solid curve). As can be seen the simulations are reasonably good in both cases, which provides support for a mechanism whereby NO• photogeneration is partially uncoupled from photogeneration of **2**.

According to the more detailed Scheme 3, recombination of **2** and NO• would initially lead back to the cage complex, which could then fragment to give **3** and 2NO• in the processes governed by k_{d2} and/or k_{cr3}. The Scheme 4 model does not allow for these possibilities, and perhaps for this reason the numerical analyses converge to different $[NO^{\bullet}]_0$ and $[\mathbf{2}]_0$ (adjustable parameter) values for the experiments carried out in the presence and absence of added reducing agent (see Supporting Information). There is no chemical reason why the presence of a reducing agent should affect the initial photoproduct distribution, so this observation highlights the limitations of the simplified model. Inclusion of a NO•-dependent dissociative pathway that converts **2**+NO• into **3**+2NO• (Scheme 4, dotted arrow) narrows the gap between the predicted parameter values, without affecting the quality of the fits (data not shown).

4. Conclusions

For photoinitiated reactions of **1** with Mb and metMb, in the presence of sufficiently high concentrations of $[Ru(NH_3)_6]^{2+}$ or $[Fe(CN)_6]^{4-}$, the amount of free NO• generated varies almost linearly with $[\mathbf{1}]_{tot}$. In addition, the slope of the [NO•] vs $[\mathbf{1}]_{tot}$ line is essentially unchanged by the choice of reducing agent, and also by reductant concentration, over a fairly wide range

of concentrations. Furthermore, Mb oxidation, a side reaction that is observed when mixtures containing only **1** and Mb are irradiated,[5] was completely suppressed when $[Ru(NH_3)_6]^{2+}$ was used as the sacrificial reducing agent. This allowed nitrosylation to be studied in isolation. Thus, irradiation of mixtures containing **1**, protein and a suitable reducing agent is an excellent way of generating NO• on the microsecond time scale, in readily predictable quantities, and in the absence of confounding side products.

In the absence of a suitable reductant, the amount of free NO• generated is no longer a linear function of $[\mathbf{1}]_{tot}$; however, in the studies with metMb, heme nitrosylation was the only protein reaction seen after the laser flash. This suggests that photolysis of **1** in the absence of a reductant can still be used to generate NO• in studies of fast reactions, if the protein under investigation is not susceptible to oxidation by intermediate **2**. In our own research, we use the linear relationship for calculating the [NO•] generated in the presence of an added reducing agent.[18] For experiments performed in the absence of an added reductant, we determine the amount of NO• generated under a given set of conditions experimentally, by running standards with metMb under the same conditions.[29]

The mechanistic details for the reactions that follow photolysis of **1** are still being worked out, but Scheme 1 with the modifications shown in Scheme 3 provide a reasonable working hypothesis, that is at least qualitatively consistent with the experimental data, under a variety of conditions. Moreover, the shapes of the experimental data sets can be reproduced using the simplified Scheme 4, whose primary mechanistic similarity to Scheme 3 is that it uncouples the formation of free NO• from that of free **2**. The ultimate goal of this project is still to theoretically predict the [NO•] generated as a function of $[\mathbf{1}]_{tot}$, in both the presence and absence of added reducing agent. To this end, future work will focus on obtaining direct experimental evidence for the existence of transient species **1b** and **1c**, to see what role if any they have in determining the final free [NO•]. We are also currently doing calculations to predict theoretically the spin delocalization expected in species **2**, which in turn should lead to predictions of the relative amounts of **1**, **1b** and **1c** that may be expected when NO• recombines with **2**.

Acknowledgment. We gratefully acknowledge helpful discussions with Prof. Alan Schwabacher, and Messrs. Nathan Ernster and Tom Lawton (all from UWM).

Supporting Information Available: Determination of the effective path lengths in the laser photoinitiated experiments. Detailed error analysis of the data. Analysis of the d[**2**]/d*t* dependence on $[Ru^{II}]$ and $[Fe^{II}]$. Details of the procedures used to numerically model the data using the Scheme 4 mechanism. All of the raw concentration vs time traces for the data that resulted in Figures 1, 3, 5, 7 and 8. The fitting of very weak spectral changes. This information is available free of charge via the internet at http://pubs.acs.org.

References and Notes

(1) Namiki, S.; Arai, T.; Fujimori, K. *J. Am. Chem. Soc.* **1997**, *119*, 3840−3841.
(2) Namiki, S.; Kaneda, F.; Ikegami, M.; Arai, T.; Fujimori, K.; Asada, S.; Hama, H.; Kasuya, Y.; Goto, K. *Bioorg. Med. Chem.* **1999**, *7*, 1695−1702.
(3) Yoshida, M.; Masashi, I.; Namiki, S.; Arai, T.; Fujimori, K. *Chem. Lett.* **2000**, 730−731.
(4) Cabail, M. Z.; Lace, P. J.; Uselding, J.; Pacheco, A. A. *J. Photochem. Photobiol. A Chem.* **2002**, *152*, 109−121.
(5) Bodemer, G.; Ellis, L. M.; Lace, P. J.; Mooren, P. E.; Patel, N. K.; Ver, Haag, M.; Pacheco, A. A. *J. Photochem. Photobiol. A Chem.* **2004**, *163*, 53−60.
(6) Hibbs, J. B.; Vavrin, Z.; Taintor, R. R. *J. Immunol.* **1987**, *138*, 550−565.
(7) Moncada, S.; Palmer, R. M. J.; Higgs, E. A. *Biochem. Pharmacol.* **1989**, *38*, 1709−1715.
(8) Bult, H.; Boeckxstaens, G. E.; Pelckmans, P. A.; Jordaens, F. H.; Van Maercke, Y. M.; Herman, A. G. *Nature* **1990**, *345*, 346−347.
(9) Shibuki, K.; Okada, D. *Nature* **1991**, *349*, 326−328.
(10) Bredt, D. S.; Hwang, P. M.; Glatt, C. E.; Lowenstein, C.; Reed, R. R.; Snyder, S. H. *Nature* **1991**, *351*, 714−718.
(11) Heck, D. E.; Laskin, D. L.; Gardner, C. R.; Laskin, J. D. *J. Biol. Chem.* **1992**, *267*, 21277−21280.
(12) Ford, P. C.; Lorkovic, I. M. *Chem. Rev.* **2002**, *102*, 993−1017.
(13) McCleverty, J. A. *Chem. Rev.* **2004**, *104*, 403−418.
(14) Bourassa, J.; DeGraff, W.; Kudo, S.; Wink, D. A.; Mitchell, J. B.; Ford, P. C. *J. Am. Chem. Soc.* **1997**, *119*, 2853−2860.
(15) De Leo, M.; Ford, P. C. *J. Am. Chem. Soc.* **1999**, *121*, 1980−1981.
(16) Hou, Y.; Xie, W.; Janczuk, A. J.; Wang, P. G. *J. Org. Chem.* **2000**, *65*, 4333−4337.
(17) Cabail, M. Z.; Pacheco, A. A. *Inorg. Chem.* **2003**, *42*, 270−272.
(18) Cabail, M. Z.; Kostera, J.; Pacheco, A. A. *Inorg. Chem.* **2005**, *44*, 225−231.
(19) Codd, R.; Astashkin, A. V.; Pacheco, A.; Raitsimring, A. M.; Enemark, J. H. *J. Biol. Inorg. Chem.* **2002**, *7*, 338−350.
(20) Press, W. H.; Teukolsky, S. A.; Vetterling, W. T.; Flannery, B. P. *Numerical Recipes in C: The Art of Scientific Computing*, 2nd ed.; Cambridge University Press: Cambridge, U.K., 1992; Chapter 15, pp 59−70.
(21) Strang, G. *Linear Algebra and Its Applications*, 3rd ed.; Harcourt Brace Jovanivich, Inc.: San Diego, CA, 1988; pp 153−162.
(22) Laverman, L. E.; Wanat, A.; Oszajca, J.; Stochel, G.; Ford, P. C.; van Eldik, R. *J. Am. Chem. Soc.* **2001**, *123*, 285−293.
(23) Laidler, K.; Meiser, J. H. *Physical Chemistry*, 2nd ed.; Houghton Miflin Co.: Boston, MA, 1995; p 388.
(24) Hoshino, M.; Ozawa, K.; Seki, H.; Ford, P. C. *J. Am. Chem. Soc.* **1993**, *115*, 9568−9575.
(25) Hoshino, M.; Maeda, M.; Konishi, R.; Seki, H.; Ford, P. C. *J. Am. Chem. Soc.* **1996**, *118*, 5702−5707.
(26) Bard, A. J.; Faulkner, L. R. *Electrochemical Methods, Fundamentals and Applictions*, 2nd ed.; John Wiley and Sons, Inc.: New York, NY, 2001; pp 808−809.
(27) Shikama, K. *Chem. Rev.* **1998**, *98*, 1357−1373.
(28) Cotton, F. A.; Wilkinson, G.; Murillo, C. A.; Bochmann, M. *Advanced Inorganic Chemistry*, 6th ed.; John Wiley and Sons, Inc.: New York, 1999; p 326
(29) Cabail, M. Z. Ph.D. Dissertation, The University of Wisconsin−Milwaukee, Milwaukee, WI, 2006.